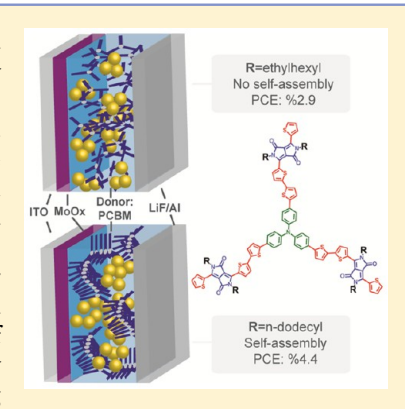
pubs.acs.org/JPCC

# Self-Assembling Tripodal Small-Molecule Donors for Bulk **Heterojunction Solar Cells**

Taner Aytun, †,‡ Peter J. Santos, †,‡ Carson J. Bruns, Dongxu Huang, † Andrew R. Koltonow, † Monica Olvera de la Cruz, †, $\$,\bot,\parallel$  and Samuel I. Stupp $*,\dagger,\$,\parallel,\#,\bigcirc$ 

Supporting Information

ABSTRACT: The power conversion efficiency of organic solar cells (OSCs) could benefit from systematic studies to improve bulk heterojunction (BHJ) morphology by modifying donor compounds. Supramolecular self-assembly is an attractive strategy to combine the beneficial properties of polymeric donors, such as a well-controlled morphology, with the homogeneous composition of small molecule donors for OSCs. We report here on two tripodal "star-shaped" small-molecule donor compounds based on diketopyrrolopyrrole (DPP) side chains for solution-processed BHJ OSCs. The tripod molecules were found not to aggregate in solution or form crystalline domains in thin films when a branched alkyl chain (2-ethylhexyl) substituent was used, whereas linear (docedecyl) alkyl chains promote the formation of one-dimensional (1D) nanowires and more crystalline domains in the solid state. We demonstrate that the 1D self-assembly of these tripods enhances the performance of the corresponding solution-processed OSCs by 50%, which is attributed to the significant increase in the fill factor of devices resulting from a reduction of trap states.



## INTRODUCTION

Solution-processed bulk heterojunction (BHJ) organic photovoltaic (OPV) materials remain under intensive investigation after almost 2 decades of fundamental research driven by their potential to bring low-cost, lightweight, flexible solar-to-electric energy conversion devices to market. 1-4 OPV power conversion efficiencies (PCEs) have been rising steadily, now exceeding 9%. The active layer of a BHJ OSC typically utilizes a fullerene-based acceptor (n-type) material in a phaseseparated blend with polymeric or small-molecule organic donor (p-type) material. The morphological elements of the active layer's p-n heterojunction include the topology of its percolation network, domain sizes, distribution of trap sites, and spatial orientation of molecules. These features collectively play a critical role in the physical phenomena that ultimately lead to charge extraction.8 Research efforts to increase OPV PCEs often involve controlling BHJ morphology through covalent modification of the donor compounds or optimization of processing conditions, 10 (e.g., thermal annealing, 11 solvent vapor annealing, 12,13 solvent additives 14). These two factors influence the process of spinodal decomposition during formation of the active layer. An alternative strategy for controlling active layer morphology is the use of programmed self-assembly in an attempt to control molecular organization within the active layer at specific length scales. 15,16 There have been several strategies used to promote self-assembly of donor molecules in solution, including discotic liquid crystals, 17,18 nematic liquid crystals, 19 liquid crystalline polymers, 20 nanostructured block copolymers, <sup>21</sup> bimolecular crystals, <sup>22</sup> hydrogen bonded networks, <sup>23</sup> and one-dimensional (1D) nanostructures.<sup>24</sup> Our group has focused recently on the use of small molecule donors that assemble into 1D nanofibers for OSCs in order to form high interfacial area percolated networks when blended with fullerenes.<sup>25</sup>

Small molecules with linear architecture have been used to create devices with efficiencies of 6%-9%. 28-33 Several "starshaped" donors with more complex architectures (C-3 symmetric or tripodal) have also been reported, with efficiencies that have now surpassed 4%. We envisioned that the increased  $\pi$ - $\pi$  stacking interactions of these disc-like molecules would promote fiber assembly when appended with alkyl side chains for solubility. We chose diketopyrrolopyrrole (DPP) units flanked by thiophene groups to serve as the chromophoric "arms" of our tripods because of DPP's favorable optoelectronic properties and well-established use in efficient  $\stackrel{\circ}{\mathrm{OPVs}}$ .  $^{27,32,39}$  We designed tripodal donor molecules  $T_{EH}$  (with 2-ethylhexyl) and T<sub>C12</sub> (with dodecyl) (Figure 1a) in which an electron-donating triphenylamine (TPA) unit serves as the

Received: October 14, 2015 Revised: January 27, 2016

<sup>&</sup>lt;sup>†</sup>Department of Materials Science and Engineering, <sup>§</sup>Department of Chemistry, <sup>⊥</sup>Department of Chemical and Biological Engineering, Department of Physics and Astronomy, and Department of Biomedical Engineering, Northwestern University, Evanston, Illinois 60208, United States

<sup>&</sup>lt;sup>#</sup>Department of Medicine and <sup>O</sup>Simpson Querrey Institute for BioNanotechnology, Northwestern University, Chicago, Illinois 60611, United States

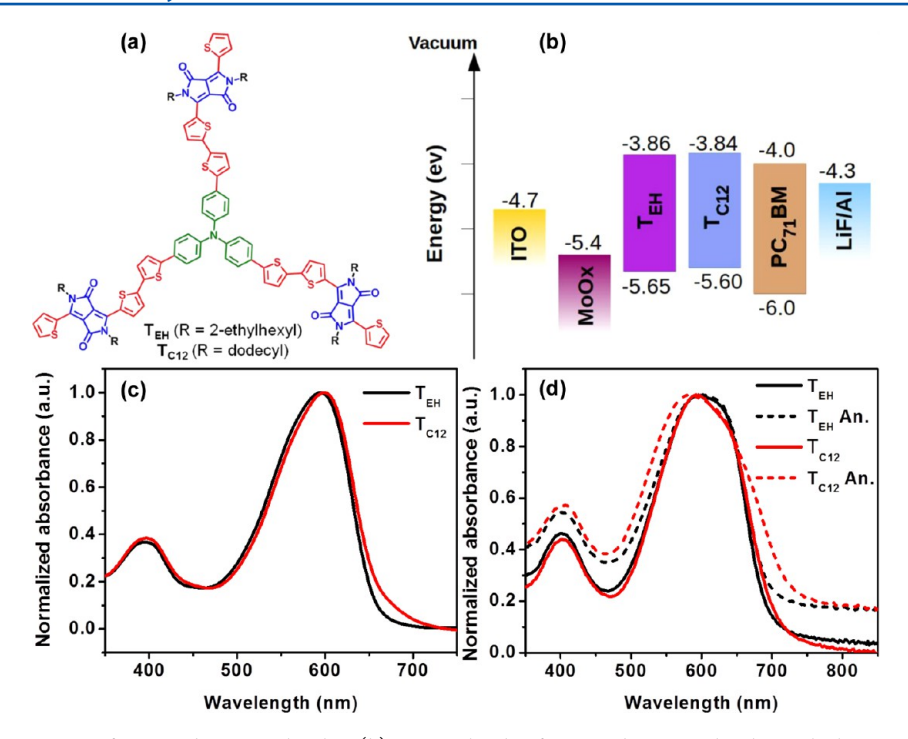


Figure 1. (a) Chemical structure of  $T_{EH}$  and  $T_{C12}$  molecules. (b) Energy levels of  $T_{EH}$  and  $T_{C12}$  molecules with the energy levels of other device layers. (b) Absorption spectra of  $T_{EH}$  and  $T_{C12}$  in chloroform solution and (d) in solid film cast from chloroform before and after annealing.

central trifurcated core. 40 A recent study by Giuseppone and co-workers has shown that TPA exhibits a remarkable propensity to form fibers and conduct charge carriers via the generation and sharing of free radicals upon photoexcitation.<sup>41</sup> While several tripodal molecules incorporating similar TPA-DPP designs have been reported for OPVs, 42,43 there was no indication that they self-assemble into well-defined nanostructures. A similar set of tripodal molecules with the 2-ethylhexyl groups and differing number of thiophenes was recently reported and yielded devices with PCEs as high as 2.95%. The true potential of tripodal chromophore solar cells will not be realized until the role of self-assembly in determining the morphology and performance is understood. In this work we investigate the influence of side chains on molecular packing of TPA-DPP tripods and therefore solar cell performance. As a complement to T<sub>EH</sub>, we study a related new tripod molecule, T<sub>C12</sub>, with straight side chains that will not interfere with molecular packing. The dodecyl (C12) side chain is used because shorter straight chains were not able to solubilize the molecule enough to form homogeneous thin films and working devices.

#### EXPERIMENTAL SECTION

**Materials and Methods.** DPPC<sub>12</sub> and N(PhTsnBu<sub>3</sub>)<sub>3</sub> were prepared according to published literature procedures. All solvents and reagents were purchased from commercial suppliers (Aldrich, Matrix Scientific) and used without further purification, with the exceptions of N-Bromosuccinimide (NBS), which was recrystallized from water. All reactions were carried out under an inert atmosphere of N<sub>2</sub>. Analytical thin-layer chromatography (TLC) was performed on aluminum sheets, precoated with silica gel 60-F<sub>254</sub> (Merck 5554). Flash column chromatography was carried out using silica gel 60 (Silicycle) as the stationary phase.

**Experimental Details.** NMR spectra were recorded on a Bruker Avance III 500 spectrometer with working frequencies

of 500 MHz for <sup>1</sup>H and 125 MHz for <sup>13</sup>C. Chemical shifts are reported in ppm and referenced to the residual nondeuterated solvent frequencies (CDCl<sub>3</sub>:  $\delta$  7.27 ppm for <sup>1</sup>H,  $\delta$  77.0 ppm for <sup>13</sup>C. Mass spectra were obtained on a Bruker Autoflex III MALDI mass spectrometer. Ultraviolet-visible (UV-vis) spectra were recorded on a PerkinElmer LAMBDA 1050 spectrophotometer. Photovoltaic measurements were recorded while the devices were illuminated by an Oriel Xe solar simulator equipped with and Oriel 130 monochromator and a Keithley 2400 source meter. Filters were used to cut off grating overtones. The solar spectrum was simulated using an AM 1.5 filter with 100 mW·cm<sup>-2</sup> power density. A calibrated silicon reference solar cell with a KG5 filter certified by the National Renewable Energy Laboratory was used to confirm the measurement conditions. AFM characterization was performed using a Bruker Dimension ICON atomic force microscope (Bruker Co.) at ambient conditions. Tapping mode was utilized with single-beam silicon cantilevers with a nominal oscillation frequency of 300 kHz. GIXD measurements were performed at Beamline 8ID-E of the Advanced Photon Source at Argonne National Laboratory. An X-ray wavelength of  $\lambda = 1.6868$  Å was used and data were collected using a 1-2 s exposure at a sample—detector distance of 204 mm with a Pilatus photodiode array. Impedance spectroscopy measurements were carried out on an AUTOLAB [PGSTAT128N with the FRA32 module for EIS] electrochemical system.

**Synthesis and Characterization.** *TDPP*<sub>C12</sub>-*Br*. Protected from light, NBS (558 mg, 3.14 mmol) in CHCl<sub>3</sub> (50 mL) was added to a solution of **TDPP**<sub>C12</sub> (2.5 g, 3.9 mmol) in CHCl<sub>3</sub> (100 mL) at 0 °C. The reaction was stirred at ambient temperature overnight and the solvent was removed under reduced pressure using rotary evaporator. The residue was subjected to flash column chromatography on SiO<sub>2</sub> (hexanes—DCM, 2:1) to afford the title compound as a purple solid (625 mg, 22%). <sup>1</sup>H NMR (500 MHz, CDCl<sub>3</sub>, 298 K):  $\delta$  = 8.94 (d, J = 3.9 Hz, 1H), 8.68 (d, J = 4.1 Hz, 1H), 7.66 (d, J = 4.9 Hz,

1H), 7.29 (dd, J = 4.7, 4.2 Hz, 1H), 7.25 (d, J = 4.3 Hz, 2H), 4.07 (t, J = 7.9 Hz, 2H), 4.00 (t, J = 7.6 Hz, 2H), 1.79–1.68 (m, 6H), 1.47–1.37 (m, 6H), 1.37–1.21 (m, 36H), 0.89 (t, J = 6.8 Hz, 3H). <sup>13</sup>C NMR (125 MHz, CDCl<sub>3</sub>, 298 K):  $\delta$  = 161.3, 161.1, 140.5, 138.5, 135.5, 135.1, 131.5, 131.2, 131.0, 129.7, 128.7, 118.8, 107.9, 107.6, 42.3, 42,2, 31.9, 30.0, 30.0, 29.9, 29.6, 29.6, 29.5, 29.5, 29.3, 29.2, 29.2, 26.9, 26.8, 22.7, 14.1. MS (MALDI) m/z, with no matrix: calcd for  $C_{38}H_{55}BrN_2O_2S_2$  [M + H]<sup>+</sup>, 716.890; found, 716.955.

 $T_{C12}$ . Dry toluene (10 mL) and dry DMF (5 mL) were added to N(PhTSnBu<sub>3</sub>)<sub>3</sub> and TDPP<sub>C12</sub>-Br (175 mg, 0.245 mmol) and degassed with  $N_2$ .  $Pd(PPh_3)_4$  (10.0 mg, 8.66  $\mu$ mol) was added and the reaction was heated to 120 °C and stirred for 24 h. The reaction mixture was poured into MeOH (150 mL), and the resulting precipitate was collected by vacuum filtration and chromatography was carried on SiO<sub>2</sub> (PhMe-CHCl<sub>3</sub>, gradient from 50:50 to 0:100). The blue solid was recrystallized by slow vapor diffusion of EtOAc into CHCl<sub>3</sub> to afford the title compound as a shiny, blue solid (83 mg, 14%). <sup>1</sup>H NMR (500 MHz, CDCl<sub>3</sub>, 298 K):  $\delta$  = 8.96 (d, J = 4.2 Hz, 3H), 8.93 (d, J = 3.9 Hz, 3H), 7.64 (d, J = 5.1 Hz, 3H), 7.56 (d, J = 8.6 Hz, 6H), 7.36 (d, J = 4.1 Hz, 3H), 7.33 (d, J = 3.7 Hz, 3H), 7.29 (dd, J =4.48 Hz, 4.10 Hz, 3H), 7.25 (d, J = 3.9 Hz, 3H), 7.20 (d, J = 9.1 HzHz, 6H), 4.10 (t, J = 7.5 Hz, 12H), 1.84-1.73 (m, 12H), 1.5-1.2, (m, 108H), 0.87 (t, J = 6.8 Hz, 9H), 0.85 (t, J = 6.8 Hz, 9H). <sup>13</sup>C NMR (125 MHz, CDCl<sub>3</sub>, 298 K):  $\delta$  = 161.4, 161.2, 146.8, 143.1, 139.6, 139.4, 136.7, 135.1, 134.7, 130.6, 129.8, 128.7, 128.6, 127.8, 126.7, 126.3, 124.7, 124.5, 123.6, 116.4, 107.9, 107.9, 42.3, 42.2, 31.9, 29.9, 29.6, 29.6, 29.6, 29.5, 29.5, 29.3, 29.2, 29.2, 26.8, 22.7, 14.1. MS (MALDI) m/z, with dithranol matrix: calcd for  $C_{144}H_{183}N_7O_6S_9H$  [M + H]<sup>+</sup>, 2397.658; found, 2397.636

**Device Fabrication.** Experimental conditions for active later deposition such as solvent, concentration and solvent composition were optimized. Prepatterned indium-doped tin oxide (ITO) on glass was used as the transparent bottom electrode. The ITO was scrubbed with soapy water and cleaned by ultrasonicating sequentially in hexanes, soapy water, water, and a 1:1:1 solution of acetone/methanol/2-propanol. The electrode was then blown dry in a N2 stream and transferred into a  $N_2$  glovebox ( $O_2$  and  $H_2O < 0.1$  ppm). Before active layer coating,  $MoO_x$  (10 nm) was thermally evaporated on ITO surface as the interfacial layer. Bulk heterojunction photovoltaic devices were fabricated from blends of donor small molecule and acceptor phenyl- $C_{71}$ -butyric acid methyl ester ( $PC_{71}BM$ ). In the optimized conditions, the donor/acceptor ratio is fixed at 1:2 for the  $T_{C12}$  molecules and 1:3 for  $T_{EH_{\rm i}}$  with a total solution concentration of 13.5 mg/mL for T<sub>C12</sub> and 16 mg/mL for T<sub>EH</sub> in chloroform. Films were cast by spin-coating at 1500 rpm for  $T_{C12}$  and 4000 rpm for  $T_{EH}$  in the glovebox for 60 s with no thermal annealing for  $T_{C12}$  and 5 min of annealing on a hot plate at 100 °C for T<sub>EH</sub>. Total organic layer thickness ranged from 90 to 100 nm as determined by AFM. Devices were completed by thermally evaporating 1 nm of LiF then 100 nm of Al through a shadow mask at  $1 \times 10^{-6}$  mbar to yield devices of 4 mm<sup>2</sup> in area and sealed with a UV-curable epoxy if needed. The devices for space-charge-limited-current (SCLC) measurements were fabricated with a similar procedure. The top electrode was replaced with Au (50 nm) rather than LiF/Al in order to suppress electron injection.

#### RESULTS AND DISCUSSION

**Synthesis and Characterization.** The tripodal donors were synthesized by Stille cross coupling of tris(4-(5-(tributylstannyl)thiophen-2-yl)phenyl)amine and monobrominated thiophene-flanked DPP compounds (BrTDPP) with 2-ethylhexyl (EH) or dodecyl (C12) side-chains to afford  $T_{EH}$  and  $T_{C12}$ , respectively. Detailed synthetic procedures can be found in the experimental section. Variations with hexyl (C6) and octyl (C8) side chains were made as well, but were found to be unsuitable for device work due to poor solubility.

In order to study the impact of self-assembly on solar device performance, two homologous molecules,  $T_{EH}$  and  $T_{C12}$  (see Figure 1a), were synthesized. These were found to have similar electronic and optical properties. The highest occupied molecular orbital (HOMO) levels were calculated by ultraviolet photoelectron spectroscopy (UPS) (see the Supporting Information for details), and the band gaps were calculated from the onset of thin film UV-vis absorption spectra.  $T_{EH}$  has a HOMO of -5.65 eV relative to vacuum level, and  $T_{C12}$  has a similar one of -5.60 eV. The HOMO levels of both compounds show slight offsets from MoO<sub>x</sub>, which is favorable for hole transport out of the active layer. The band gaps of  $T_{EH}$ and T<sub>C12</sub> are 1.79 and 1.76 eV, respectively. The compounds show offsets from the lowest unoccupied molecular orbital (LUMO) of PC<sub>71</sub>BM of 0.16 and 0.14 eV. As can be seen in Figure 1b, the energy levels of the two compounds are comparable, and their small offsets to PC71BM are favorable for effective exciton splitting. The UV-vis absorption spectra of T<sub>EH</sub> and T<sub>C12</sub> in CHCl<sub>3</sub> (Figure 1c) confirm that the optical properties between the two molecules are analogous (both with extinction coefficients higher than 10<sup>5</sup> M<sup>-1</sup>cm<sup>-1</sup>). T<sub>EH</sub> shows an absorption maximum at 595 nm and T<sub>C12</sub> at 598 nm, and they both absorb up to wavelengths of approximately 700 nm. We also observed some differences in the absorption spectra of the two tripods as thin films spin coated from CHCl<sub>3</sub> (Figure 1d). The absorption maximum of the  $T_{EH}$  film is red-shifted, while that of  $T_{C12}$  is blue-shifted relative to the solution spectra. Both of these shifts are magnified upon annealing. The red-shift in the case of T<sub>EH</sub> indicates the formation of J-aggregates involving the stacking of T<sub>EH</sub> molecules in an end-to-end manner. Similarly, the blue-shift can be attributed to the formation of H-aggregates, providing evidence for the cofacial stacking of T<sub>C12</sub> molecules in the film. Additionally, a shoulder in the  $T_{C12}$  film at 670 nm most likely arises from J-aggregate formation involved in nanowire bundling. The optical properties of the compounds are summarized in Table 1.

Table 1. Optical Properties of Solutions and Films of Tripod Molecules

	solution $\lambda_{\max}$ (nm)	$\lim_{\lambda_{\max} (nm)}$	film annealed $\lambda_{\max}$ (nm)	$E_{\rm g} ({\rm eV})^a$	$\varepsilon$ at $\lambda_{\text{max}} \times 10^5$ (M <sup>-1</sup> cm <sup>-1</sup> )
$T_{EH}$	595	596	600	1.79	1.7
$T_{C12} \\$	598	592	584	1.76	1.3

Supramolecular Self-Assembly of Tripodal Molecules.

<sup>a</sup>Measured from the onset of the absorbance of the film.

The assembly of the tripodal molecules was further characterized by atomic force microscopy (AFM) and grazing incidence X-ray diffraction (GIXD). AFM topography and phase images in Figure 2a and Figure 2d show that  $T_{\rm EH}$  forms featureless films when cast from chloroform, even after annealing for 5 min at 120 °C. Conversely, Figure 2b and

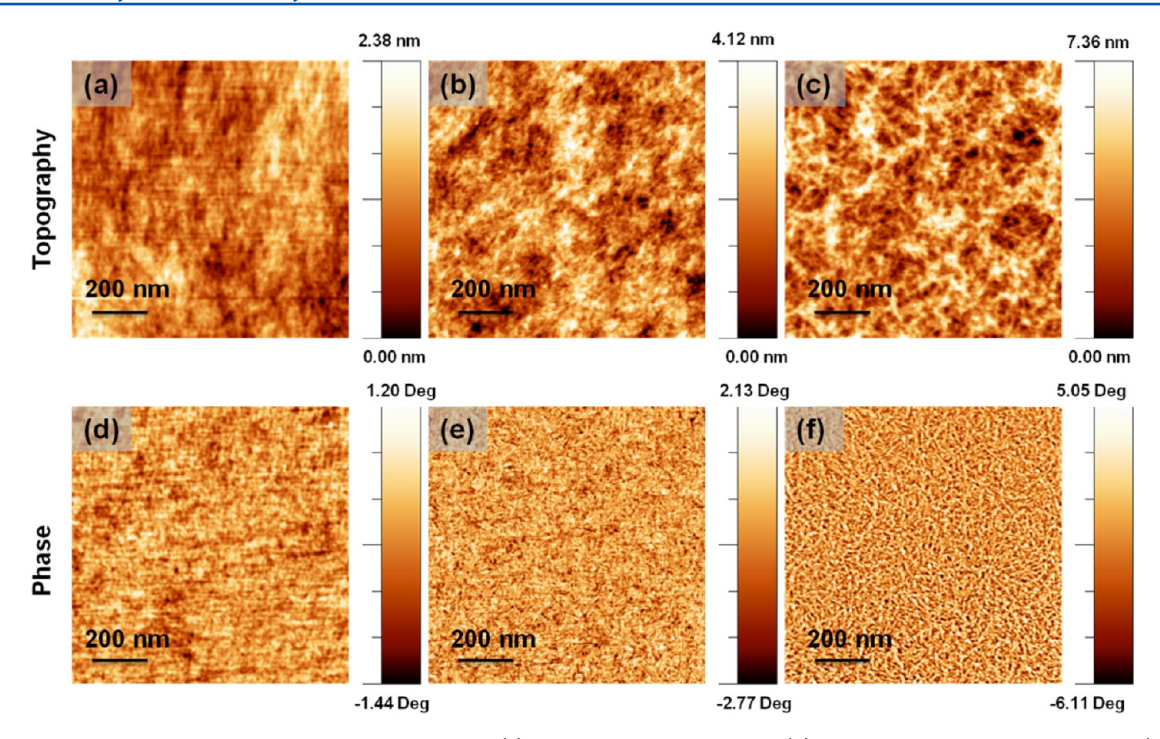


Figure 2. AFM topography images of  $T_{EH}$  cast from chloroform (a),  $T_{C12}$  cast from chloroform (b), and  $T_{C12}$  cast from chlorobenzene (c), with the corresponding phase images (d-f), respectively.

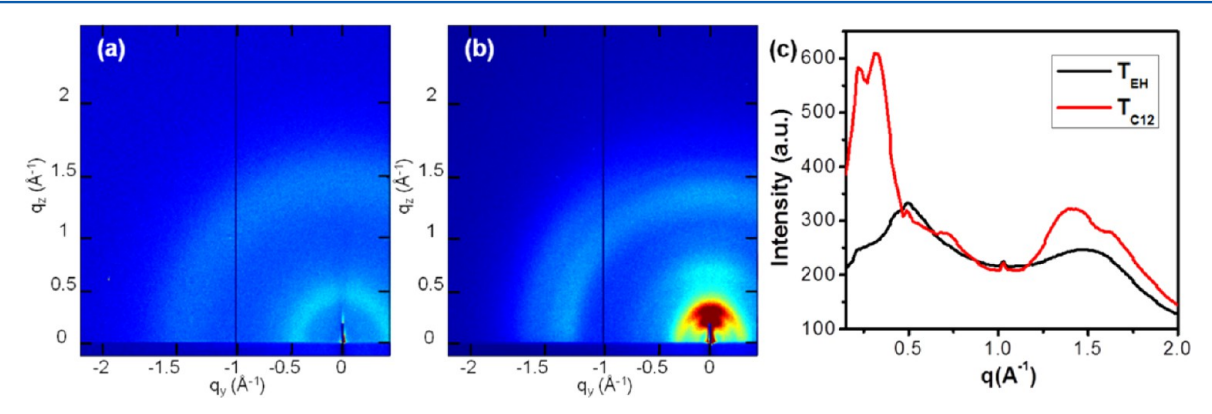


Figure 3. GIXD of  $T_{EH}$  (a) and  $T_{C12}$  (b) drop cast from chloroform. (c) Line profiles of GIXD data for  $T_{EH}$  and  $T_{C12}$ .

Figure 2e show that  $T_{C12}$  forms short nanowires when cast under same conditions. When a  $T_{C12}$  solution is cast from chlorobenzene, the self-assembly of the nanowire morphology is further enhanced, as shown in Figure 2c and Figure 2f. The height of the nanowires in Figure 2c is around 2.5–3 nm, which scales with the molecular diameter of  $T_{C12}$  molecules. On the other hand, there was no such morphology change for  $T_{EH}$  when it was cast from chlorobenzene (Figure S6).

2D GIXD data collected from films of the tripodal molecules are shown in Figure 3. A  $T_{EH}$  film drop cast from chloroform and slowly dried produces diffuse and weak diffraction rings (Figure 3a). The ring around 0.5 Å<sup>-1</sup> corresponds to a 1.3 nm distance, which can be attributed to the center-to-center distance when one arm of each molecule overlaps. The ring around 1.47 Å<sup>-1</sup> corresponds to 0.43 nm, which can arise from the cofacial packing of each arm of adjacent molecules in a stack. This spacing is greater than what is expected for  $\pi$ – $\pi$  stacking distances (~0.37 nm) in conjugated small molecules. In addition, neither of the diffuse rings have a directional preference with respect to the substrate. We conclude that the

 $T_{EH}$  molecules do not self-organize with a significant order parameter. On the other hand,  $T_{C12}$  films prepared under similar conditions exhibit diffraction rings with much higher intensities (Figure 3b). Two distinct rings at 0.22 Å<sup>-1</sup> (2.9 nm) and 0.31 Å<sup>-1</sup> (2.0 nm) appear in the low q region (Figure 3c). The 2.9 nm distance can be attributed to the center-to-center spacing between two adjacent nanowires, in agreement with AFM observations. The ring around 1.4 Å<sup>-1</sup> (0.45 nm) is similar to  $T_{EH}$  but in this case there is a small hump in the line profile around 1.6 Å<sup>-1</sup> (0.38 nm) which is very close to conventional  $\pi$ - $\pi$  stacking distances. In summary, GIXD results show that  $T_{C12}$  molecules tend to organize with cofacial stacking to a greater extent than  $T_{EH}$  molecules, which is consistent with the "nanowire" morphologies observed by AFM.

To support this hypothesis, a classical molecular dynamics (MD) simulation was performed with Groningen machine for chemical structures (GROMACS) package. The objective of the simulation was to compare the relative ordering capacity in solution of the two donor molecules investigated here. We

carried this out using explicit solvent molecules since interaction potentials for MD are parametrized against solvent environments. In vacuum, we would expect to predict an overly packed structure. The simulations were therefore done in water and chloroform.

The final supramolecular structures predicted by the simulations of the two molecules are shown in Figure 4a and

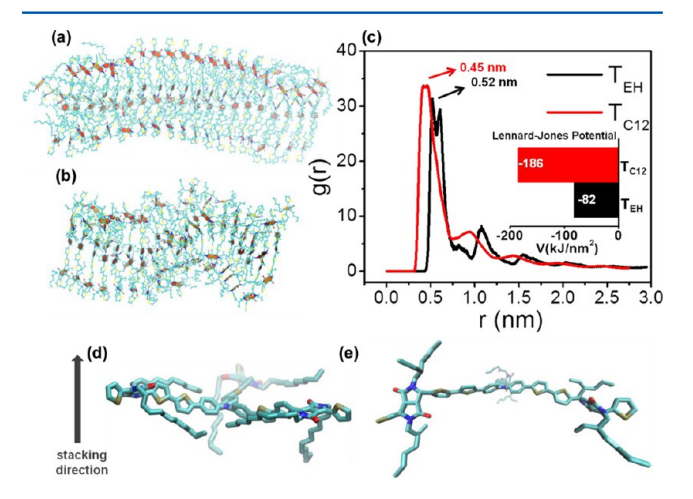


**Figure 4.** MD simulation of stacked (a)  $T_{C12}$  and (b)  $T_{EH}$  and (c) radial distribution function of the molecules with an inset of Lennard-Jones potential values. Single molecules from the MD stacking simulation for (d)  $T_{C12}$  and (e)  $T_{EH}$ .

Figure 4b.  $T_{C12}$  shows ordering and alignment of molecules in the assembly, while  $T_{EH}$  exhibits a significant degree of disorder. Moreover,  $T_{C12}$  molecules appear from the simulation to be much less challenged by sterics along the stacking direction (Figure 4d) relative to  $T_{EH}$  molecules (Figure 4e). We

have quantified further the ordering stability in both supramolecular systems using the intermolecular radial distribution functions (RDF) shown in Figure 4c. The RDF of T<sub>C12</sub> assemblies contains sharper and more intense peaks than that of the  $T_{EH}$  system indicating a higher local density of  $\pi$ - $\pi$ stacking. The peaks of the  $T_{C12}$  compound yield an intermolecular spacing of 0.45 nm compared to 0.52 nm for T<sub>EH</sub>. One might expect that the larger spacing between molecules predicted by the simulation relative to GIXD data can be attributed to the explicit use of a solvent environment. Also, a degree of periodicity can be observed in the peaks of T<sub>C12</sub>, which provides further evidence of the stronger interactions  $T_{C12}$  relative to  $T_{EH}$ . The Leonard-Jones energy calculations are shown in the inset in Figure 4c, quantifying the relative strengths of noncovalent interactions in the two systems,  $-186 \text{ kJ/nm}^2$  for  $T_{C12}$  and  $-82 \text{ kJ/nm}^2$  for  $T_{EH}$ .

Morphology of the Active Layer. AFM was utilized to evaluate the morphology of active layer films containing donor molecules and PC71BM as the electron acceptor. Chloroform was used as the solvent for devices because the limited solubility of T<sub>C12</sub> in chlorobenzene resulted in devices with lower efficiencies. As shown in Figure 5, parts a and d, T<sub>EH</sub>:PC<sub>71</sub>BM cast from chloroform without any additives forms predominantly flat, featureless films. Two solvent additives were used in this study, 1,8-diiodooctane (DIO) and *m*-cresol (MC). DIO is a high boiling point solvent additive that is known to solubilize PC71BM, and therefore allows the film to reach a more crystalline morphology by slowing the precipitation of the fullerene phase. 49 MC was used to increase the solubility of the donor molecule. Upon the addition of DIO, the root-meansquare (RMS) roughness of the film increases from 0.3 to 1.2 nm (Figure 5b), but the phase image (Figure 5e) indicates that the film remains homogeneous without any obvious sign of textures resulting from supramolecular self-assembly. The

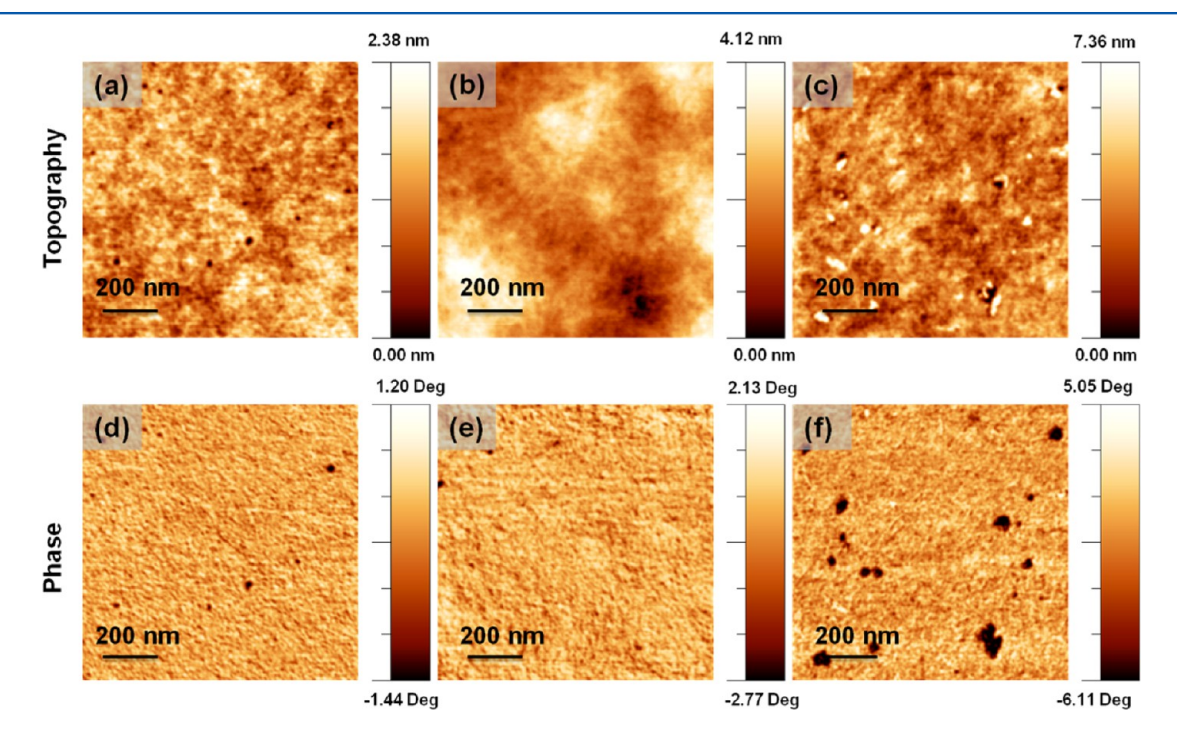


**Figure 5.** AFM topography and phase images of films created with the T<sub>EH</sub> donor. Parts a and d are, respectively, the height and phase image of the material without any solvent additives, parts b and e have 0.8 volume percent DIO, and parts c and f contain both the same amount of DIO and 1.0 volume percent *m*-cresol.

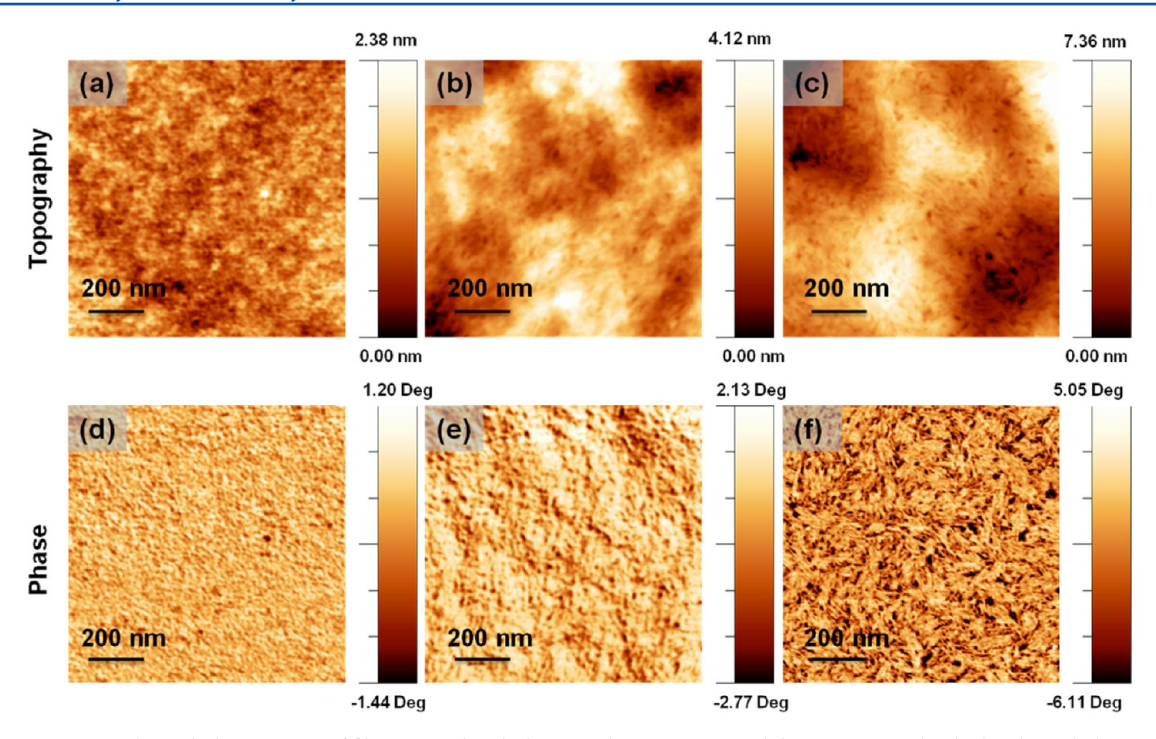


**Figure 6.** AFM topography and phase images of films created with the T<sub>C12</sub> donor. Parts a and d are, respectively, the height and phase image of the material without any solvent additives, parts b and e, have 0.8 volume percent DIO, and parts c and f contain both the same amount of DIO and 1.0 volume percent *m*-cresol.

Table 2. Optimized Solar Cell Results of Tripod Molecules with PC71BM

sample	$J_{\rm sc}~({\rm mA\cdot cm}^2)$	$V_{\rm oc}$ (V)	FF (%)	PCE (%)	$R_{\rm sh}~(\Omega\cdot{\rm cm}^2)$	$R_{\rm s}~(\Omega{\cdot}{\rm cm}^2)$		
$T_{EH}:PC_{71}BM$	7.78	0.89	35	$2.41 (2.34)^a$	212	30		
T <sub>EH</sub> :PC <sub>71</sub> BM with DIO	8.61	0.87	37	2.75 (2.63)	167	22		
$T_{EH}$ :PC <sub>71</sub> BM with DIO + MC	8.95	0.89	36	2.91 (2.82)	200	27		
$T_{C12}$ :PC $_{71}$ BM	4.92	0.83	32	1.29 (1.23)	230	57		
T <sub>C12</sub> :PC <sub>71</sub> BM with DIO	10.10	0.73	57	4.19 (4.04)	322	8		
$T_{C12}$ :PC <sub>71</sub> BM with DIO + MC	10.17	0.75	58	4.39 (4.26)	390	9		
<sup>a</sup> Average PCE of four devices.								

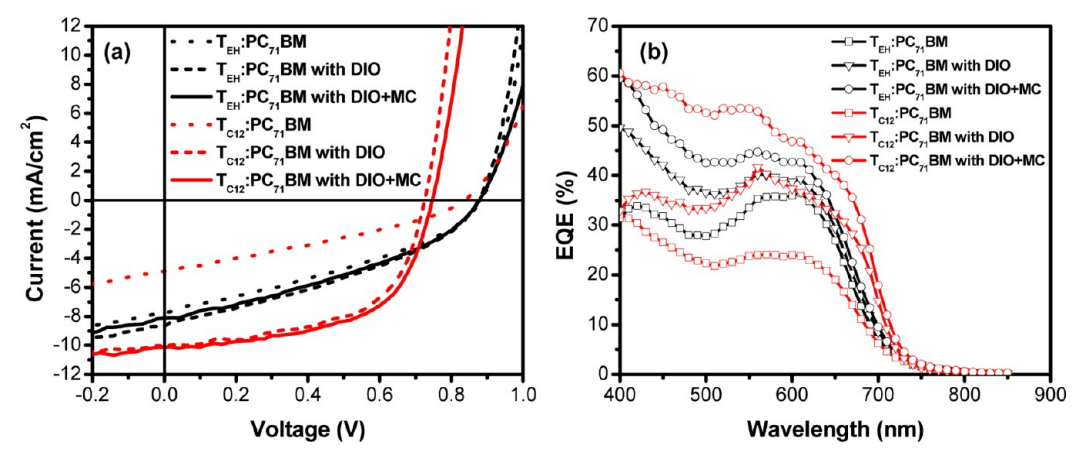


Figure 7. (a) J-V characteristics of optimized organic solar cells of tripod molecules with PC<sub>71</sub>BM under illumination (AM 1.5). (b) External quantum efficiency (EQE) of the same devices.

incorporation of MC as a solvent additive flattens the film (Figure 5c), returning the roughness to 0.3 nm, but does not induce any obvious nanoscale organization (Figure 5f).  $T_{C12}$ :PC<sub>71</sub>BM films (Figure 6a) are equally featureless in the absence of any solvent additives. Although  $T_{C12}$  forms small nanowires in chloroform, it forms featureless films after

blending with  $PC_{71}BM$  (Figure 6d). One of the reasons for this could be that  $PC_{71}BM$  disrupts the stacking of tripodal molecules. Another reason could be that chloroform leaves the film quickly during the spin coating process and does not provide enough time for  $T_{C12}$  molecules to stack effectively. However, the incorporation of DIO increases both the

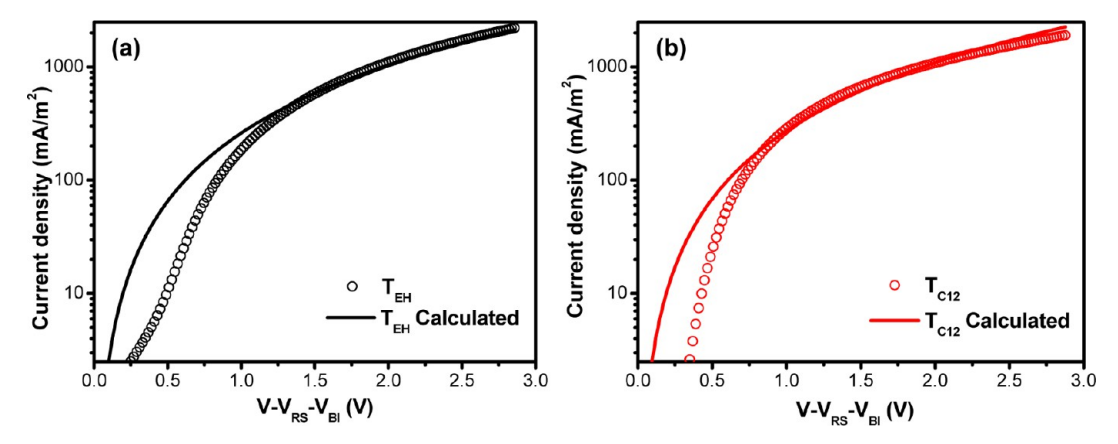


Figure 8. Experimental dark-current densities measured at room temperature in a hole-only device configuration (open circles) superimposed with curves calculated from SCLC theory (solid lines) for (a)  $T_{EH}$ :PC<sub>71</sub>BM with DIO + MC and (b)  $T_{C12}$ :PC<sub>71</sub>BM with DIO + MC.

roughness of the film from 0.3 to 2.6 nm (Figure 6b) and creates large, seemingly amorphous features in the phase image (Figure 6e). The aggregates that appear in the phase image are potentially bundled nanowires that are too dense to be clearly resolved by AFM. In the third set of images, it is apparent that the combination of MC and DIO promotes assembly of  $T_{CI}$ . into a well-dispersed network of nanowires. Instead of lowering the roughness of the film as in the case of TEH, the nanowires that form in the presence of MC and DIO additives raise the RMS roughness to 3.5 nm (Figure 6c). The nanowires visible in Figure 6f are likely well-dispersed but otherwise identical to the bundles present in Figure 6e, since the UV-vis spectra of the two active layer films show the same features with minimal spectral shift (see Figure S7). GIXD characterization was also performed on the active layer blends, but few features could be resolved, indicating that the stacking of tripodal donors is disrupted by PC<sub>71</sub>BM during spin-casting (Figure S8).

Photovoltaic Properties of Tripodal Molecules. Solar cells containing  $T_{C12}$  and  $T_{EH}$  were fabricated using optimized weight ratios of donor:PC71BM of 1:2 and 1:3, respectively. Each blend used chloroform as the primary solvent. Annealing conditions for T<sub>EH</sub> and T<sub>C12</sub> devices were optimized separately. For T<sub>EH</sub>, annealing at 100 °C for 5 min resulted in the best performing devices. By contrast, the  $T_{C12}$  devices performed best when not annealed. The results of optimized devices are summarized in Table 2 and Figure 7, parts a and b, and further information on the fabricated devices can be found in the Supporting Information. Without any solvent additives, devices based on T<sub>EH</sub> show higher performance than those of T<sub>C12</sub>, with PCEs of 2.41% and 1.29%, respectively.  $T_{C12}$  exhibits slightly lower open circuit voltage  $(V_{oc})$  and significantly lower short circuit current  $(J_{sc})$  than  $T_{EH}$ . The drop in  $V_{oc}$  matches the difference in HOMO levels between the two donors, and the change in  $J_{sc}$  can be attributed to a lower solubility of the T<sub>C12</sub> donor and its longer, electrically insulating alkyl tails. The addition of 0.8 volume percent DIO, however, greatly increases the performance of both donors. As demonstrated by the AFM images (Figures 5 and 6), DIO induces the formation of molecular nanowires in the active layer for  $T_{C12}$ , which can explain the significant increase in fill factor (FF) from 0.32 to 0.54, and  $J_{sc}$  from 7.78 to 10.19 mA·cm<sup>-2</sup>. Moreover, the series resistance of  $T_{C12}$  decreases significantly from 57 to 8  $\Omega \cdot \text{cm}^2$ , while  $T_{EH}$  had a much smaller decrease from 30 to 22  $\Omega \cdot cm^2$ . Interestingly, the  $V_{oc}$  of  $T_{C12}$  devices was further depressed by the addition of DIO. This decrease can be attributed to the

assembly of the nanowires with long alkyl tails further impeding the donor-fullerene interactions and to a narrowing of the band gap and increase in the donor HOMO level on account of  $\pi$ – $\pi$ stacking. Since the two molecules show very similar optical properties, we believe the difference in performance is due to the self-assembly of  $T_{C12}$  into a supramolecular nanostructure. T<sub>EH</sub> does not form nanowires in the film, and exhibits inferior performance compared to T<sub>C12</sub> after DIO is added. The performance of the solar cells was further improved by the addition of 1.0 volume percent MC as a solvent additive, which most likely functions as a dispersant. The addition of MC increased the shunt resistance of the T<sub>EH</sub> active layer from 167 to 200  $\Omega$ ·cm<sup>2</sup>, while T<sub>C12</sub> active layers rose from 322 to 389  $\Omega$ · cm<sup>2</sup>. The fully optimized devices have a PCE of 4.39% for  $T_{C12}$ and 2.91% for  $T_{EH}$ . Our optimized results for  $T_{EH}$  are in agreement with what has been reported previously. 44 We conclude that the use of linear alkyl tails rather than branched ones promotes supramolecular self-assembly in these tripodal molecules, imparting a 50% improvement in device performance while minimally affecting the optoelectronic properties of the molecules.

Hole Mobility and Impedance Spectroscopy of Tripod **Solar Cells.** To explain the relative increase in FF for the  $T_{C12}$ devices with additives, we performed hole mobility measurements and impedance spectroscopy on active layers cast from solutions containing both solvent additives (DIO + MC). It has been shown that increases in FF are correlated with increases in hole mobility and reduction of trap states. 50 The hole mobilities of the active layers were measured for hole-only devices fabricated with gold top electrodes and using the space-charge limited current (SCLC) method.<sup>51</sup> The SCLC regime occurs at higher voltages, and so the hole mobilities were extracted from a fit of those data points, as shown in Figure 8a and Figure 8b. The hole mobility values for the  $T_{EH}$  device  $(5.2 \times 10^{-5} \text{ cm}^2 \cdot$  $V^{-1} \cdot s^{-1}$ ) and the  $T_{C12}$  device  $(4.0 \times 10^{-5} \text{ cm}^2 \cdot V^{-1} \cdot s^{-1})$  are very similar. Thus, changes in hole mobility do not explain the improved FF in the  $T_{C12}$  device. Furthermore, the device mobilities measured cannot be used to draw conclusions about differences in mobilities corresponding to the two molecules used, since this property in the device is influenced by other factors including molecular packing and alignment, nanoscale morphology, the presence of PC71BM, interfaces, and trap

In order to study the recombination kinetics of our system, impedance spectroscopy was carried out on devices under open

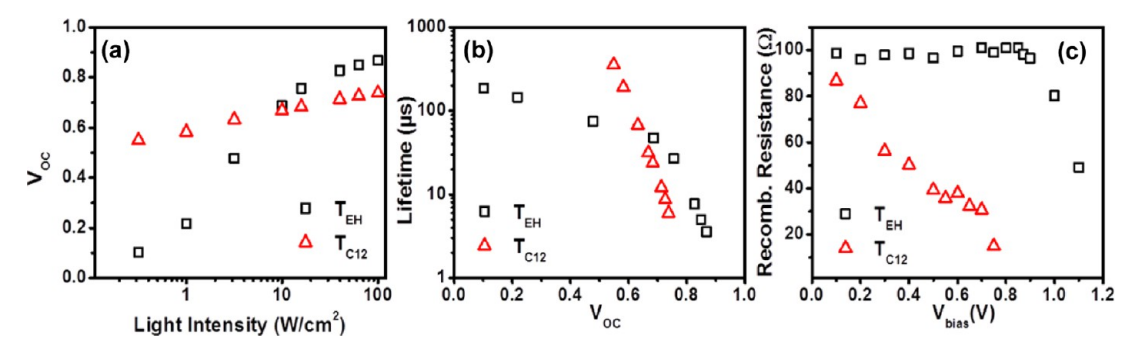


Figure 9. (a)  $V_{\rm oc}$  versus light intensity, (b) lifetime versus  $V_{\rm OC}$  (c) and recombination resistance versus applied bias ( $V_{\rm bias}$ ) of the optimized  $T_{\rm EH}$  and  $T_{\rm C12}$  devices.

circuit conditions. Upon varying the illumination, the photovoltage of the  $T_{C12}$  film scales linearly, with  $dV_{\rm oc}/d(\ln(\Phi))=1.3k_{\rm B}T/q$ , reasonably close to the expected value of unity for a system experiencing bimolecular recombination. However, the photovoltage of the  $T_{\rm EH}$  film is far more sensitive to light intensity, its slope changing from 2.4 at higher light intensities to 6.8 at lower light intensities, indicating the presence of an additional recombination mechanism (Figure 9a). Furthermore, while the carrier lifetime in the  $T_{\rm C12}$  film shows the predicted dependence on  $V_{\rm oc}$ , the carrier lifetime in the  $T_{\rm EH}$  film is nonlinear, trending toward a smaller slope at low illumination intensities (Figure 9b), which suggests that trap-mediated recombination is far more prevalent in the  $T_{\rm EH}$  film than in the  $T_{\rm C12}$  film.

The device with a larger degree of trap recombination would be expected to have a higher series resistance. When the bias is swept (Figure 9c) the series resistance of the T<sub>EH</sub> film is nearly unchanged until it dramatically decreases as the  $V_{oc}$  is approached, implying that the traps lie deep in the energy landscape of the system. In contrast, the series resistance of the  $T_{C12}$  film decreases gradually as the bias is swept, suggesting that that device's trap states are shallow and easily surmounted. On the basis of these impedance spectroscopy experiments, we conclude that trap states in the  $T_{\text{EH}}$  active layer are more numerous and deeper seated than those in the  $T_{C12}$  active layer. Therefore, the supramolecular self-assembly of  $T_{C12}$  molecules creates ordered domains, while steric effects prevent TEH molecules from stacking thus forming amorphous domains with more structural defects that may lead to electronic trap states.

### CONCLUSIONS

Two homologous tripodal small molecule electron donors with triphenylamine cores and diketopyrrolopyrrole chromophoric arms were synthesized and used to study the impact of supramolecular self-assembly on OPV performance. We found that branched alkyl solubilizing chains inhibit the self-assembly of these tripodal molecules, while linear side chains promote the self-assembly of bundled one-dimensional nanowires. The two molecules have comparable optoelectronic properties in solution and neat films, but respond differently to the addition of solvent additives. This in turn generates significantly different film morphologies and device performances. The compound with linear side chains (T<sub>C12</sub>) assembles into nanowires, and also shows a 50% increase in PCE relative to its branched counterpart (T<sub>EH</sub>) owing to a significant gain in FF. We attribute the improvement in performance to the nanowires reducing trap states in the active layer, which is supported by

impedance spectroscopy. This work demonstrates that creating supramolecular structures via self-assembly is a useful strategy for improving the photovoltaic performance of small molecules by helping to control morphology across length scales.

### ASSOCIATED CONTENT

## **S** Supporting Information

The Supporting Information is available free of charge on the ACS Publications website at DOI: 10.1021/acs.jpcc.5b10064.

Circuit model used for fitting, impedance spectroscopy, ultraviolet photoelectron spectroscopy, solar cell results, grazing incidence X-ray diffraction, and simulation results (PDF)

#### AUTHOR INFORMATION

### **Corresponding Author**

\*(S.I.S.) E-mail: s-stupp@northwestern.edu. Telephone: +1 (847) 491-3002.

#### **Author Contributions**

<sup>‡</sup>T.A. and P.J.S. contributed equally to this work.

#### Note

The authors declare no competing financial interest

## ACKNOWLEDGMENTS

This work was supported by the U.S. Department of Energy, Office of Science, Basic Energy Sciences, under Award No. DE-FG02-00ER45810 (S.I.S.) except for the computer simulation work, which was supported by Northwestern University Materials Research and Engineering Center (NU-MRSEC) funded by the NSF Under Award No. DMR-1121262 (MOC). P.J.S. acknowledges support from the Northwestern Undergraduate Summer Research Grant, the Meister Family Undergraduate Research Grant, and the McCormick Undergraduate Research Grant. A.R.K. acknowledges support by the National Science Foundation Graduate Research Fellowship under Grant No. DGE-1324585. The authors are also grateful to the following shared facilities at Northwestern University: IMSERC, Keck Biophysics, and the NIFTI facility of NUANCE Center. NUANCE Center is supported by NSF-NSEC, NSF-MRSEC, the Keck Foundation, the State of Illinois, and Northwestern University; IMSERC NMR usage under Award NSF CHE-1048773 is appreciated. Use of Advanced Photon Source sector 8-ID-E, an Office of Science User Facility operated for the U.S. Department of Energy (DOE) Office of Science by Argonne National Laboratory, was supported by the U.S. DOE under Contract No. DE-AC02-06CH11357. The authors also thank Dr. Liam Palmer for fruitful discussions and

help with the manuscript, Dr. G. Shekhawat for his help with AFM measurements and Dr. J. Strzalka for GIXD measurements at Argonne National Laboratory.

### REFERENCES

- (1) Dou, L.; You, J.; Hong, Z.; Xu, Z.; Li, G.; Street, R. A.; Yang, Y. 25th Anniversary Article: A Decade of Organic/Polymeric Photovoltaic Research. *Adv. Mater.* **2013**, *25*, 6642–6671.
- (2) Günes, S.; Neugebauer, H.; Sariciftci, N. S. Conjugated Polymer-Based Organic Solar Cells. *Chem. Rev.* **2007**, *107*, 1324–1338.
- (3) Li, W.; Furlan, A.; Hendriks, K. H.; Wienk, M. M.; Janssen, R. A. J. Efficient Tandem and Triple-Junction Polymer Solar Cells. *J. Am. Chem. Soc.* **2013**, *135*, 5529–5532.
- (4) Liu, Y.; Zhao, J.; Li, Z.; Mu, C.; Ma, W.; Hu, H.; Jiang, K.; Lin, H.; Ade, H.; Yan, H. Aggregation and Morphology Control Enables Multiple Cases of High-Efficiency Polymer Solar Cells. *Nat. Commun.* **2014**, *5*, 5293.
- (5) He, Z.; Zhong, C.; Su, S.; Xu, M.; Wu, H.; Cao, Y. Enhanced Power-Conversion Efficiency in Polymer Solar Cells Using an Inverted Device Structure. *Nat. Photonics* **2012**, *6*, 591–595.
- (6) Brabec, C. J.; Gowrisanker, S.; Halls, J. J. M.; Laird, D.; Jia, S.; Williams, S. P. Polymer–Fullerene Bulk-Heterojunction Solar Cells. *Adv. Mater.* **2010**, *22*, 3839–3856.
- (7) Mishra, A.; Bäuerle, P. Small Molecule Organic Semiconductors on the Move: Promises for Future Solar Energy Technology. *Angew. Chem., Int. Ed.* **2012**, *51*, 2020–2067.
- (8) Hoppe, H.; Sariciftci, N. S. Morphology of Polymer/fullerene Bulk Heterojunction Solar Cells. *J. Mater. Chem.* **2006**, *16*, 45–61.
- (9) Nguyen, L. H.; Hoppe, H.; Erb, T.; Günes, S.; Gobsch, G.; Sariciftci, N. S. Effects of Annealing on the Nanomorphology and Performance of Poly(alkylthiophene):Fullerene Bulk-Heterojunction Solar Cells. *Adv. Funct. Mater.* **2007**, *17*, 1071–1078.
- (10) Peet, J.; Senatore, M. L.; Heeger, A. J.; Bazan, G. C. Bulk Heterojunction Solar Cells: The Role of Processing in the Fabrication and Optimization of Plastic Solar Cells. *Adv. Mater.* **2009**, *21*, 1521–1527.
- (11) Padinger, F.; Rittberger, R. s.; Sariciftci, N. s. Effects of Postproduction Treatment on Plastic Solar Cells. *Adv. Funct. Mater.* **2003**, *13*, 85–88.
- (12) Li, G.; Shrotriya, V.; Huang, J.; Yao, Y.; Moriarty, T.; Emery, K.; Yang, Y. High-Efficiency Solution Processable Polymer Photovoltaic Cells by Self-Organization of Polymer Blends. *Nat. Mater.* **2005**, *4*, 864–868.
- (13) Wei, G.; Wang, S.; Sun, K.; Thompson, M. E.; Forrest, S. R. Solvent-Annealed Crystalline Squaraine: PC70BM (1:6) Solar Cells. *Adv. Energy Mater.* **2011**, *1*, 184–187.
- (14) Hoven, C. V.; Dang, X.-D.; Coffin, R. C.; Peet, J.; Nguyen, T.-Q.; Bazan, G. C. Improved Performance of Polymer Bulk Heterojunction Solar Cells Through the Reduction of Phase Separation via Solvent Additives. *Adv. Mater.* **2010**, *22*, E63–E66.
- (15) Beaujuge, P. M.; Fréchet, J. M. J. Molecular Design and Ordering Effects in Π-Functional Materials for Transistor and Solar Cell Applications. *J. Am. Chem. Soc.* **2011**, *133*, 20009–20029.
- (16) Wang, M.; Wudl, F. Top-down Meets Bottom-up: Organized Donor-acceptor Heterojunctions for Organic Solar Cells. *J. Mater. Chem.* **2012**, 22, 24297–24314.
- (17) Schmidt-Mende, L.; Fechtenkötter, A.; Müllen, K.; Moons, E.; Friend, R. H.; MacKenzie, J. D. Self-Organized Discotic Liquid Crystals for High-Efficiency Organic Photovoltaics. *Science* **2001**, 293, 1119–1122.
- (18) Feng, X.; Liu, M.; Pisula, W.; Takase, M.; Li, J.; Müllen, K. Supramolecular Organization and Photovoltaics of Triangle-Shaped Discotic Graphenes with Swallow-Tailed Alkyl Substituents. *Adv. Mater.* **2008**, *20*, 2684–2689.
- (19) Carrasco-Orozco, M.; Tsoi, W. C.; O'Neill, M.; Aldred, M. P.; Vlachos, P.; Kelly, S. M. New Photovoltaic Concept: Liquid-Crystal Solar Cells Using a Nematic Gel Template. *Adv. Mater.* **2006**, *18*, 1754–1758.

I

- (20) Sun, Q.; Park, K.; Dai, L. Liquid Crystalline Polymers for Efficient Bilayer-Bulk-Heterojunction Solar Cells. *J. Phys. Chem. C* **2009**, *113*, 7892–7897.
- (21) Guo, C.; Lin, Y.-H.; Witman, M. D.; Smith, K. A.; Wang, C.; Hexemer, A.; Strzalka, J.; Gomez, E. D.; Verduzco, R. Conjugated Block Copolymer Photovoltaics with near 3% Efficiency through Microphase Separation. *Nano Lett.* **2013**, *13*, 2957–2963.
- (22) Kang, S. J.; Kim, J. B.; Chiu, C.-Y.; Ahn, S.; Schiros, T.; Lee, S. S.; Yager, K. G.; Toney, M. F.; Loo, Y.-L.; Nuckolls, C. A Supramolecular Complex in Small-Molecule Solar Cells Based on Contorted Aromatic Molecules. *Angew. Chem., Int. Ed.* **2012**, *51*, 8594–8597.
- (23) Lin, Y.; Lim, J. A.; Wei, Q.; Mannsfeld, S. C. B.; Briseno, A. L.; Watkins, J. J. Cooperative Assembly of Hydrogen-Bonded Diblock Copolythiophene/Fullerene Blends for Photovoltaic Devices with Well-Defined Morphologies and Enhanced Stability. *Chem. Mater.* **2012**, *24*, 622–632.
- (24) Xin, H.; Kim, F. S.; Jenekhe, S. A. Highly Efficient Solar Cells Based on Poly(3-Butylthiophene) Nanowires. *J. Am. Chem. Soc.* **2008**, 130, 5424–5425.
- (25) Tevis, I. D.; Tsai, W.-W.; Palmer, L. C.; Aytun, T.; Stupp, S. I. Grooved Nanowires from Self-Assembling Hairpin Molecules for Solar Cells. *ACS Nano* **2012**, *6*, 2032–2040.
- (26) Ruiz-Carretero, A.; Aytun, T.; Bruns, C. J.; Newcomb, C. J.; Tsai, W.-W.; Stupp, S. I. Stepwise Self-Assembly to Improve Solar Cell Morphology. *J. Mater. Chem. A* **2013**, *1*, 11674–11681.
- (27) Aytun, T.; Barreda, L.; Ruiz-Carretero, A.; Lehrman, J. A.; Stupp, S. I. Improving Solar Cell Efficiency through Hydrogen Bonding: A Method for Tuning Active Layer Morphology. *Chem. Mater.* **2015**, *27*, 1201–1209.
- (28) Sun, Y.; Welch, G. C.; Leong, W. L.; Takacs, C. J.; Bazan, G. C.; Heeger, A. J. Solution-Processed Small-Molecule Solar Cells with 6.7% Efficiency. *Nat. Mater.* **2011**, *11*, 44–48.
- (29) Zhou, J.; Zuo, Y.; Wan, X.; Long, G.; Zhang, Q.; Ni, W.; Liu, Y.; Li, Z.; He, G.; Li, C.; et al. Solution-Processed and High-Performance Organic Solar Cells Using Small Molecules with a Benzodithiophene Unit. J. Am. Chem. Soc. 2013, 135, 8484—8487.
- (30) Kyaw, A. K. K.; Wang, D. H.; Wynands, D.; Zhang, J.; Nguyen, T.-Q.; Bazan, G. C.; Heeger, A. J. Improved Light Harvesting and Improved Efficiency by Insertion of an Optical Spacer (ZnO) in Solution-Processed Small-Molecule Solar Cells. *Nano Lett.* **2013**, *13*, 3796–3801.
- (31) Walker, B.; Tamayo, A. B.; Dang, X.-D.; Zalar, P.; Seo, J. H.; Garcia, A.; Tantiwiwat, M.; Nguyen, T.-Q. Nanoscale Phase Separation and High Photovoltaic Efficiency in Solution-Processed, Small-Molecule Bulk Heterojunction Solar Cells. *Adv. Funct. Mater.* **2009**, 19, 3063–3069.
- (32) Loser, S.; Bruns, C. J.; Miyauchi, H.; Ortiz, R. P.; Facchetti, A.; Stupp, S. I.; Marks, T. J. A Naphthodithiophene-Diketopyrrolopyrrole Donor Molecule for Efficient Solution-Processed Solar Cells. *J. Am. Chem. Soc.* **2011**, *133*, 8142–8145.
- (33) Lee, O. P.; Yiu, A. T.; Beaujuge, P. M.; Woo, C. H.; Holcombe, T. W.; Millstone, J. E.; Douglas, J. D.; Chen, M. S.; Fréchet, J. M. J. Efficient Small Molecule Bulk Heterojunction Solar Cells with High Fill Factors via Pyrene-Directed Molecular Self-Assembly. *Adv. Mater.* **2011**, *23*, 5359–5363.
- (34) De Bettignies, R.; Nicolas, Y.; Blanchard, P.; Levillain, E.; Nunzi, J.-M.; Roncali, J. Planarized Star-Shaped Oligothiophenes as a New Class of Organic Semiconductors for Heterojunction Solar Cells. *Adv. Mater.* **2003**, *15*, 1939–1943.
- (35) Ripaud, E.; Rousseau, T.; Leriche, P.; Roncali, J. Unsymmetrical Triphenylamine-Oligothiophene Hybrid Conjugated Systems as Donor Materials for High-Voltage Solution-Processed Organic Solar Cells. *Adv. Energy Mater.* **2011**, *1*, 540–545.
- (36) Hu, Z.; Li, X.; Zhang, W.; Liang, A.; Ye, D.; Liu, Z.; Liu, J.; Liu, Y.; Fang, J. Synthesis and Photovoltaic Properties of Solution-Processable Star-Shaped Small Molecules with Triphenylamine as the Core and Alkyl Cyanoacetate or 3-Ethylrhodanine as the End-Group. RSC Adv. 2014, 4, 5591–5597.

- (37) Lin, Y.; Zhang, Z.-G.; Bai, H.; Li, Y.; Zhan, X. A Star-Shaped Oligothiophene End-Capped with Alkyl Cyanoacetate Groups for Solution-Processed Organic Solar Cells. *Chem. Commun.* **2012**, 48, 9655–9657.
- (38) Min, J.; Luponosov, Y. N.; Gerl, A.; Polinskaya, M. S.; Peregudova, S. M.; Dmitryakov, P. V.; Bakirov, A. V.; Shcherbina, M. A.; Chvalun, S. N.; Grigorian, S.; et al. Alkyl Chain Engineering of Solution-Processable Star-Shaped Molecules for High-Performance Organic Solar Cells. *Adv. Energy Mater.* **2014**, *4*, 1301234.
- (39) Chandran, D.; Lee, K.-S. Diketopyrrolopyrrole: A Versatile Building Block for Organic Photovoltaic Materials. *Macromol. Res.* **2013**, *21*, 272–283.
- (40) Thelakkat, M. Star-Shaped, Dendrimeric and Polymeric Triarylamines as Photoconductors and Hole Transport Materials for Electro-Optical Applications. *Macromol. Mater. Eng.* **2002**, 287, 442–461
- (41) Faramarzi, V.; Niess, F.; Moulin, E.; Maaloum, M.; Dayen, J.-F.; Beaufrand, J.-B.; Zanettini, S.; Doudin, B.; Giuseppone, N. Light-Triggered Self-Construction of Supramolecular Organic Nanowires as Metallic Interconnects. *Nat. Chem.* **2012**, *4*, 485–490.
- (42) Lin, Y.; Cheng, P.; Li, Y.; Zhan, X. A 3D Star-Shaped Non-Fullerene Acceptor for Solution-Processed Organic Solar Cells with a High Open-Circuit Voltage of 1.18 V. Chem. Commun. 2012, 48, 4773–4775.
- (43) Pan, J.-Y.; Zuo, L.-J.; Hu, X.-L.; Fu, W.-F.; Chen, M.-R.; Fu, L.; Gu, X.; Shi, H.-Q.; Shi, M.-M.; Li, H.-Y.; et al. Star-Shaped D—A Small Molecules Based on Diketopyrrolopyrrole and Triphenylamine for Efficient Solution-Processed Organic Solar Cells. ACS Appl. Mater. Interfaces 2013, 5, 972—980.
- (44) Tang, A.; Li, L.; Lu, Z.; Huang, J.; Jia, H.; Zhan, C.; Tan, Z.; Li, Y.; Yao, J. Significant Improvement of Photovoltaic Performance by Embedding Thiophene in Solution-Processed Star-Shaped TPA-DPP Backbone. J. Mater. Chem. A 2013, 1, 5747–5757.
- (45) Hess, B.; Kutzner, C.; van der Spoel, D.; Lindahl, E. GROMACS 4: Algorithms for Highly Efficient, Load-Balanced, and Scalable Molecular Simulation. *J. Chem. Theory Comput.* **2008**, *4*, 435–447.
- (46) Autiero, I.; Saviano, M.; Langella, E. Molecular Dynamics Simulations of PNA-PNA and PNA-DNA Duplexes by the Use of New Parameters Implemented in the GROMACS Package: A Conformational and Dynamics Study. *Phys. Chem. Chem. Phys.* **2014**, *16*, 1868–1874
- (47) Keasar, C.; Rosenfeld, R. Empirical Modifications to the Amber/OPLS Potential for Predicting the Solution Conformations of Cyclic Peptides by Vacuum Calculations. *Folding Des.* **1998**, *3*, 379–388.
- (48) Norin, M.; Haeffner, F.; Hult, K.; Edholm, O. Molecular Dynamics Simulations of an Enzyme Surrounded by Vacuum, Water, or a Hydrophobic Solvent. *Biophys. J.* **1994**, *67*, 548–559.
- (49) Su, M.-S.; Kuo, C.-Y.; Yuan, M.-C.; Jeng, U.-S.; Su, C.-J.; Wei, K.-H. Improving Device Efficiency of Polymer/Fullerene Bulk Heterojunction Solar Cells Through Enhanced Crystallinity and Reduced Grain Boundaries Induced by Solvent Additives. *Adv. Mater.* **2011**, 23, 3315–3319.
- (50) Proctor, C. M.; Love, J. A.; Nguyen, T.-Q. Mobility Guidelines for High Fill Factor Solution-Processed Small Molecule Solar Cells. *Adv. Mater.* **2014**, *26*, 5957–5961.
- (51) Mihailetchi, V. D.; van Duren, J. K. J.; Blom, P. W. M.; Hummelen, J. C.; Janssen, R. A. J.; Kroon, J. M.; Rispens, M. T.; Verhees, W. J. H.; Wienk, M. M. Electron Transport in a Methanofullerene. *Adv. Funct. Mater.* **2003**, *13*, 43–46.
- (52) Bisquert, J.; Mora-Seró, I. Simulation of Steady-State Characteristics of Dye-Sensitized Solar Cells and the Interpretation of the Diffusion Length. *J. Phys. Chem. Lett.* **2010**, *1*, 450–456.
- (53) Guerrero, A.; Ripolles-Sanchis, T.; Boix, P. P.; Garcia-Belmonte, G. Series Resistance in Organic Bulk-Heterojunction Solar Devices: Modulating Carrier Transport with Fullerene Electron Traps. *Org. Electron.* **2012**, *13*, 2326–2332.